Advanced Powder Technology 28 (2017) 785–797

Contents lists available at ScienceDirect

Advanced Powder Technology

journal homepage: www.elsevier.com/locate/apt

Original Research Paper

Facile green synthesis of zinc oxide nanoparticles by *Eucalyptus globulus* and their photocatalytic and antioxidant activity

Siripireddy Balaji, Mandal Badal Kumar *

Trace Elements Speciation Research Laboratory, Department of Chemistry, School of Advanced Sciences, VIT University, Vellore 632014, India

ARTICLE INFO

Article history:
Received 11 February 2016
Received in revised form 2 September 2016
Accepted 22 November 2016
Available online 7 January 2017

Keywords:
Eucalyptus globulus
ZnO NPs
Photocatalytic and antioxidant activity
DPPH

ABSTRACT

Eucalyptus globulus leaf extract mediated synthesis of spherical zinc oxide nanoparticles (ZnO NPs) was carried out under ambient conditions. UV–Visible studies of the synthesized nanoparticles revealed the characteristic peak at 361 nm indicating the formation of ZnO nanoparticles. Powder X-ray Diffractometric (XRD) study showed the strong, intense and narrow-width diffraction peaks indicating the formation of crystalline nanoparticles with most stable hexagonal phase. Field emission-scanning electron microscopy (FE-SEM) and high resolution-transmission electron microscopic (HR-TEM) results confirmed the formation of spherical ZnO NPs with mean particle size of 11.6 nm which is in close agreement with XRD pattern. Further, energy dispersive X-ray diffraction analysis (EDAX) revealed the formation of highly pure ZnO NPs with the peaks of Zn and O atoms. ZnO NPs exhibited effective photocatalytic activity in degrading Methylene blue and Methyl orange with maximum degradation efficiency up to 98.3% at 30 mg of catalyst doses. In addition, ZnO NPs exhibited high antioxidant activity against DPPH free radicals scavenger.

1. Introduction

Most dyes released by the industries such as plastic, leather, paint, food, tanneries, pharmaceutical, cosmetic and textile industries belong to mainly synthetic organic compounds. During last decades the discharge of effluents from industries containing intractable pollutants causes severe concern and challenge to our environment. The color content in dye absorbs and reflects sunlight radiation by inflowing polluted water, thereby hindering photosynthesis and interfere the development of aqua species [1]. Dyes contain different functional groups like acidic, basic, azo, anthraquinone and metal complexes. Most of the dyes cause a major health problem in humans including mutagenic and carcinogenic effects. These organic pollutants may induce skin irritation, a blood disorder, liver and kidney damage with the poisoning of the central nervous system in humans and animals [2,3]. Dyes cannot be degraded readily by predictable methods such as coagulation, flocculation, adsorption on activated carbon and membrane filtration. Conversion of these compounds to non-toxic compounds is difficult due to complex structures and higher stability. In order to overcome these difficulties researchers are favoring green synthesized metal oxide NPs for the degradation of organic contaminants as a green catalyst [4] due to the involvement of environmentally non-toxic reactants, solvents and without any unwanted byproducts during synthesis [5]. In addition, for safe operation, energy saving and avoiding the use of organic solvents, the development of suitable processes for the degradation of organic dyes in aqueous solutions under the mild condition is still in demand for both industrially and environmentally. Since the conventional methods involve toxic chemicals and produce toxic intermediates which are hazardous to the environment, green methods promote the researchers to minimize the usage of toxic chemicals and reduce waste generation by doing operations in aqueous medium [6]. Among different metal oxides NPs ZnO NPs has gained lot of importance due to its versatile properties. ZnO NPs exhibits hexagonal phase, wurtzite structure with a wide band gap of 3.37 eV and n-type semiconductor [7]. ZnO nanostructures are used in optoelectronic devices such as liquid crystal devices, solar cells, piezoelectric, metal insulator-semiconducting diodes and catalytic applications [8,9]. The fabrication of ZnO NPs is dominated by various physical and organic methods such as thermal evaporation, pulsed layer deposition, molecular beam epitaxy and chemical vapor condensation (CVC) [10–12]. Generally, these methods consuming supplementary energy and obligatory high vacuum, whereas chemical methods such as chemical vapor

* Corresponding author. Fax: +91 4162243092.
E-mail addresses: badalmandal@vit.ac.in, badalkmandal@gmail.com (B.K. Mandal).

http://dx.doi.org/10.1016/j.apt.2016.11.026
0921-8831/

deposition (CVD), sol-gel, hydrothermal, spray pyrolysis, sonochemical and electro-deposition methods are costly and harmful mass production methods [13,14].

Biological fabrication of ZnO NPs by using plants, microorganisms, algae and enzymes are ecologically favorable and sustainable compared to physical and chemical approaches [15]. Although significant works had been reported on using various plant-based extracts to formulate several metal oxide nanoparticles, the use of *Eucalyptus globulus* (*E. globulus*) plant extract mediated biosynthesis of ZnO nanoparticles explicitly is not seen in literature. *E. globulus* (Blue gum) is an evergreen tree native to Australia and also found in other southeast countries. *E. globulus* leaves are widely used in Ayurveda and general public community due to its divergent health promoting medicinal activity effects against respiratory and cold infections [16–18].

Present work reports the green synthesis of ZnO NPs by using *E. globulus* as green reducing and capping agent for the first time to our knowledge. The crystal structure, surface morphology, and sizes are characterized by using UV–Visible spectroscopy, PXRD, FE-SEM, HR-TEM, DLS techniques. The efficiency of ZnO nanoparticles as photocatalyst for the degradation of various organic dyes like methylene blue and methyl orange and their antioxidant activity by DPPH assay are studied (see Table 1).

2. Experimental section

2.1. Materials

Fresh leaves of *E. globulus* were collected in the early morning during the month of March 2015 in the University of Hyderabad (UOH) Campus, Hyderabad [19]. Zinc nitrate hexahydrate [$Zn(NO_3)_2{\cdot}6H_2O$] and required organic solvents were purchased from Sigma-Aldrich, India. De-ionized Milli-Q water was used throughout the experiments.

2.2. Preparation of extract

Freshly collected leaves were washed 2–3 times under running tap water and sanitized with Milli-Q water 2–3 times and dried at room temperature in dust free condition for one week. Fully dried leaves were crushed into powder form by using an electrical mixer. About 20 g of leaf powder was added to 100 ml of de-ionized water and kept for boiling at 80 °C for about 1 h. The appearance of the light black color solution was observed which settled down at room temperature. The formed precipitate was filtered and the obtained supernatant was stored at 4 °C in the refrigerator for further use.

Table 1
Catalytic doses of ZnO NPs for degradation of methylene blue and methyl orange dyes.

Dye name and Conc. (M)	Weight of the catalyst (mg)	Time (min)	Degradation (%)
Methylene blue 10^{-4} (M)	5	180	96
	10	160	96.8
	15	125	97.2
	20	90	97.5
	25	50	98.3
Methyl orange 10^{-4} (M)	5	185	95.0
	10	162	95.8
	15	136	96.2
	20	105	96.5
	25	83	97.0
	30	60	97.3

2.3. Synthesis of zinc oxide nanoparticles

Required amount of precursor $Zn(NO_3)_3{\cdot}6H_2O$ was dissolved in de-ionized water to prepare 0.1 N 20 mL solutions after stirring for some time. Then 20 mL of *E. globulus* plant leaves extract was mixed with 20 mL precursor solution in equal ratio (1:1 v/v) drop by drop with the aid of peristaltic pump stirring at 600 rpm for 3 h till the formation of a brown colored precipitate and allowed to settle for 24 h. The solution was centrifuged at 6000 rpm for 15 min and finally washed 2–3 times with ethanol to remove impurities followed by drying at 80 °C in hot air oven for 24 h. Dried ZnO NPs powder was exposed to annealing in a muffle furnace at 400 °C for 2 h.

2.4. Characterization

The formed ZnO NPs powder was characterized by using powder X-ray Diffractometer (PXRD) (SMART Bruker D8 Advance X-ray Diffractometer) with Cu Kα radiation (λ = 1.5404 Å) after scanning at 2θ from 20° to 90° and at an accelerating voltage of 40 kV for determining crystallinity and size of crystallites/nanoparticles. The surface morphology and chemical composition i.e. purity were determined by using FE-SEM with Energy dispersive X-ray spectroscopy (EDX) (FE-SEM, Carl-Zeiss model ultra-microscope 55, Germany) at 30 kV electron beam energy. Transmission electron microscopic (TEM) studies (FEI-make electron microscope TECNAI G2 S-Twin) were carried out at an accelerating voltage of 200 kV. Electron diffraction patterns (EDP) and selected area electron diffraction (SAED) were recorded using Gatan CCD camera. Raman spectral analysis was performed by using Senterra R200-L apparatus (Bruker Optics) by passing laser light with a wavelength of 532 nm. Dynamic light scattering and Zeta potential studies were done using Horiba Scientific Nano particci (SZ-100) instrument to identify the particle size distribution and hence the stability of nanoparticles. Specific surface area, average pore diameter and pore volume were measured using Autosorb-1 instrument (Quanta Chrome Nova-1000 Instrument). The Brunauer-Emmett-Teller (BET) specific surface area of samples was measured by adsorption-desorption study of nitrogen molecules at 77 K. Barrett-Joyner-Halenda (BJH) method was used to measure the pore size distribution derived from desorption isotherms. UV-DRS (UV-Diffuse Reflectance mode) studies were conducted by using UV–Vis-NIR spectrophotometer (JASCO-V-670) to find out the band gap energy values at a wavelength range from 200 nm to 800 nm. To identify metal–oxygen bond interactions and functional moieties studies were performed by Attenuated Total Reflection-Fourier Transform Infrared spectrometer (ATR-FTIR) (ATR-FTIR, Jasco-4100) at wave number range from 4000 to 400 cm^{-1}. The chemical compounds present in *E. globulus* extract were identified by Gas chromatography–Mass spectroscopic (GC–MS) analysis using Clarus 680 electron ionization model (Perkin Elmer, India) and controlled by Turbo mass version 5.4.2 software. The GC–MS employed a fused silica column (packed with Elite-5MS (5% biphenyl 95% dimethyl polysiloxane, 30 m × 0.25 mm ID × 250 μm df) and the components were separated by using helium as inert carrier gas at a constant flow rate of 1 mL min^{-1} and scan time interval of 0.1 s with run time of 60 min. The spectra of the components were compared with the aid of NIST database (2008) library and identified.

2.5. Adsorption study

Batch tests for adsorption of MB and MO dyes by ZnO NPs as adsorbent were performed under normal room conditions in absence of UV light. Separate batch experiments were carried out for MB and MO in the absence of both ZnO NPs and UV light. In

brief, 50 mL of aqueous MB and MO dye solution (10 mg L^{-1}) was taken in Carson tube with or without ZnO NPs and shaken at 50 rpm under room temperatures for 50 and 60 min by a rotospin-test tube rotor (Tarsons-India). After filtration using a micro filtration assembly (Millipore, Bedford, MA, USA) with 0.2 μm membrane filter paper the absorbance was measured at different time intervals using UV–Vis spectrophotometer to check the progress of adsorption with time.

2.6. Photocatalytic activity

Efficiency of photocatalytic degradation of methylene blue (MB) and methyl orange (MO) in aqueous solution using synthesized ZnO NPs was determined in a photoreactor (Heber multi-lamp photoreactor HML MP 88) equipped with mercury lamp (8 W, 0.170 Å) and input power voltage was 220–230 V at 50 Hz under UV light irradiation (λ 254 nm). In the present experiment, 50 mL of both MB and MO aqueous dye solution (10 mg L^{-1}) was taken in a quartz tube with different amount of catalyst (5, 10, 15, 20, 25 and 30 mg) for degradation study and was stirred for 30 min in the dark before irradiation. The progress of the reaction was monitored by using UV–visible spectrophotometer at different time intervals. Blue and orange color of the dyes gradually decreased and turned into colorless solution within 50 and 60 min. Absorbance peak of MB at 665 nm and that of MO at 460 nm disappeared within 50 and 60 min indicating the synthesized ZnO NPs exhibited effective photocatalytic activity in degrading both the dyes.

2.7. Antioxidant activity

The antioxidant activity of ZnO NPs was carried out by Brand Williams's method [20] using DPPH (1,1 Diphenyl-2-picryl hydrazyl) assay to determine the percentage of scavenging capacity. In the present experiment 1 mL of 50% methanol along with various concentrations of the test sample and standard ascorbic acid were added to the 1 mL of 1 mM DPPH in small test tube incubated at 37 °C under dark conditions up to 30 min and then absorbance was recorded at 517 nm by using UV–visible spectrophotometer. Generally, DPPH liberates free radicals and ZnO NPs scavenges the free radicals inhibiting its antioxidant activity. Percentage of inhibition values were calculated by using standard ascorbic acid absorbance values. The difference in absorbance readings between control (DPPH) and the test sample was calculated to determine the IC_{50} (Half maximal inhibitory concentration) values.

3. Results and discussion

In the present work, we synthesized stable crystalline zinc oxide nanoparticles through one step process without using any external surfactant (or) chemical stabilizer. In addition, we got uniform spherical NPs of 11.6 nm size which are smaller than the ZnO NPs synthesized by other chemical and green methods [21–30] (Table ST2). Basically, plant extracts act as size controlling agent who prevents nucleation and coalescence of NPs i.e. regulate the aggregation or agglomeration of NPs or crystallites. The following

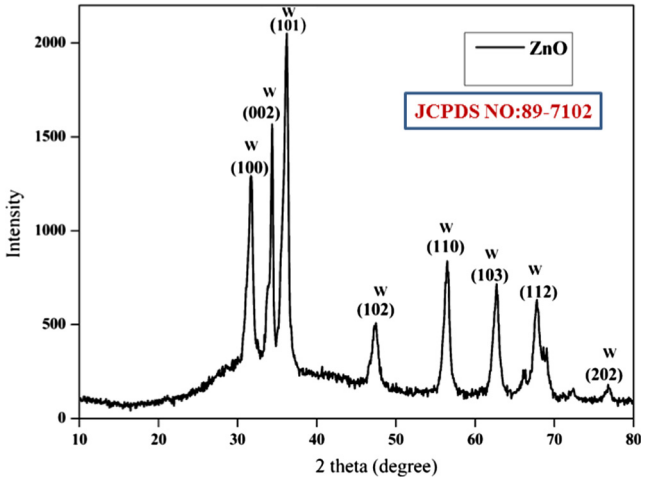

Fig. 2. XRD pattern of synthesized ZnO NPs.

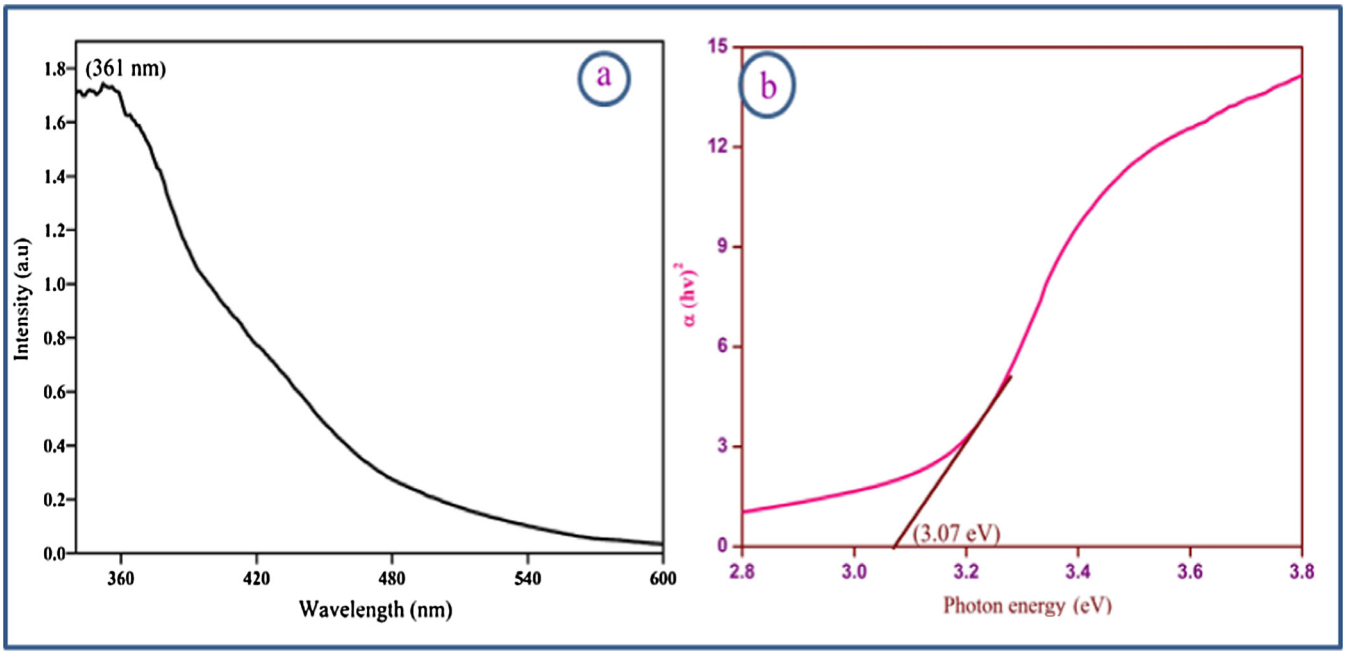

Fig. 1. (a) UV–visible absorption spectra of synthesized ZnO NPs by using *Eucalyptus globulus* plant extract (b) UV-DRS plot of ZnO NPs.

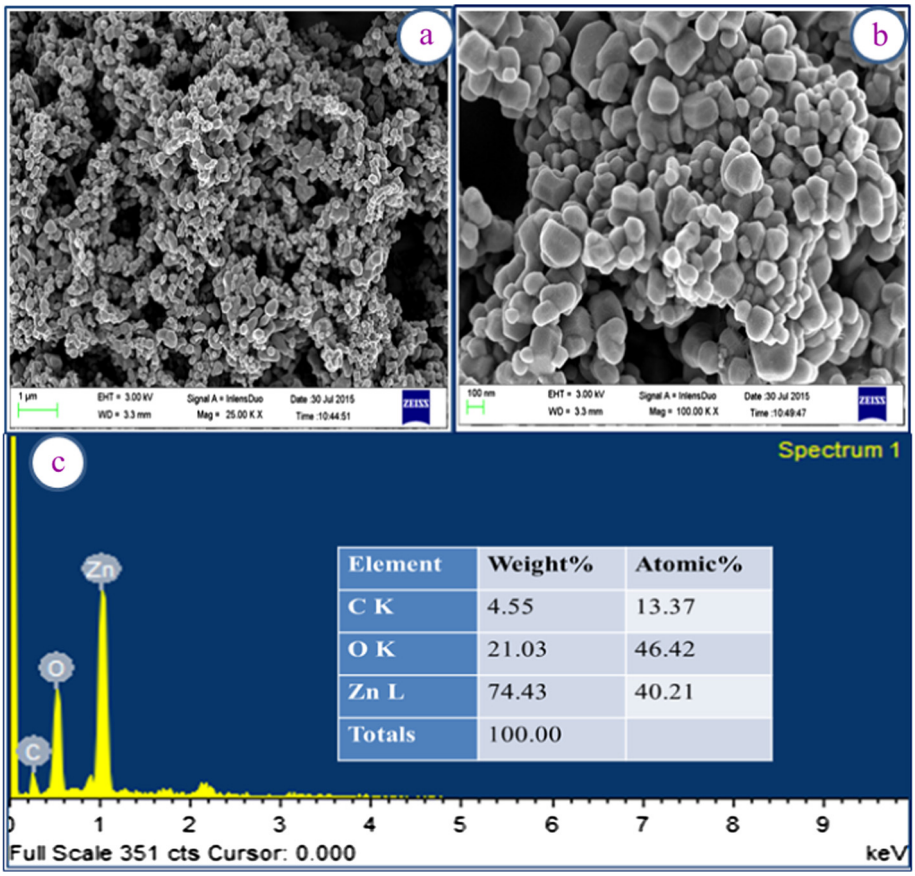

Fig. 3. FE-SEM images of ZnO NPs at different magnifications (a) 1 μm magnification, (b) 100 nm magnification and (C) EDX spectrum of synthesized ZnO NPs.

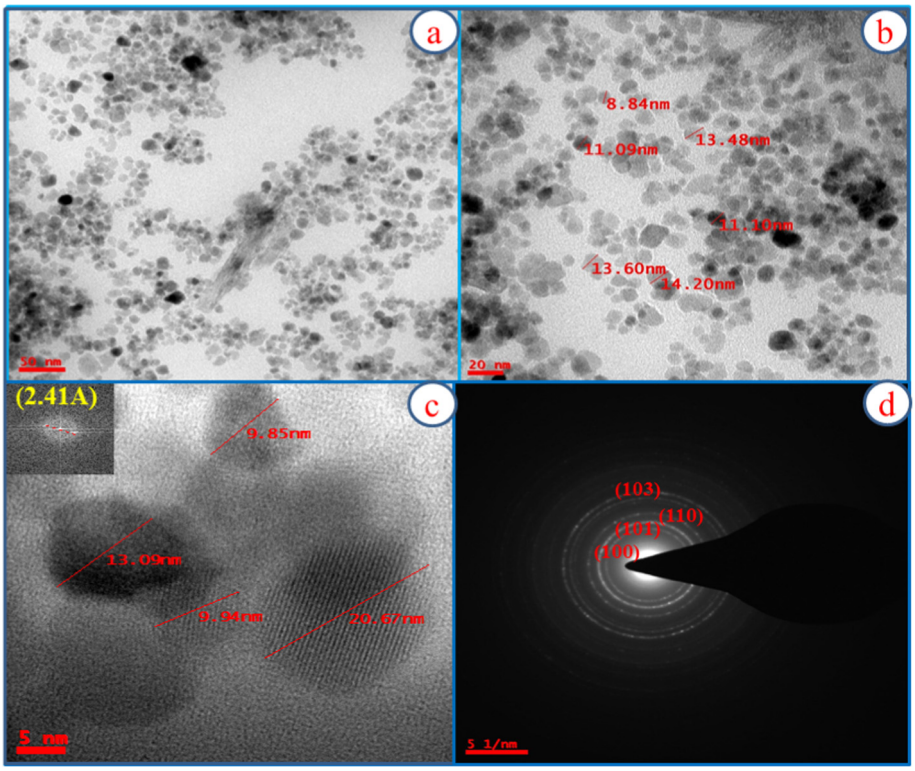

Fig. 4. TEM images of ZnO NPs at different magnifications (a) 50 nm, (b) 20 nm, (c) HR-TEM image of ZnO NPs at 5 nm and (d) SAED pattern of synthesized ZnO NPs.

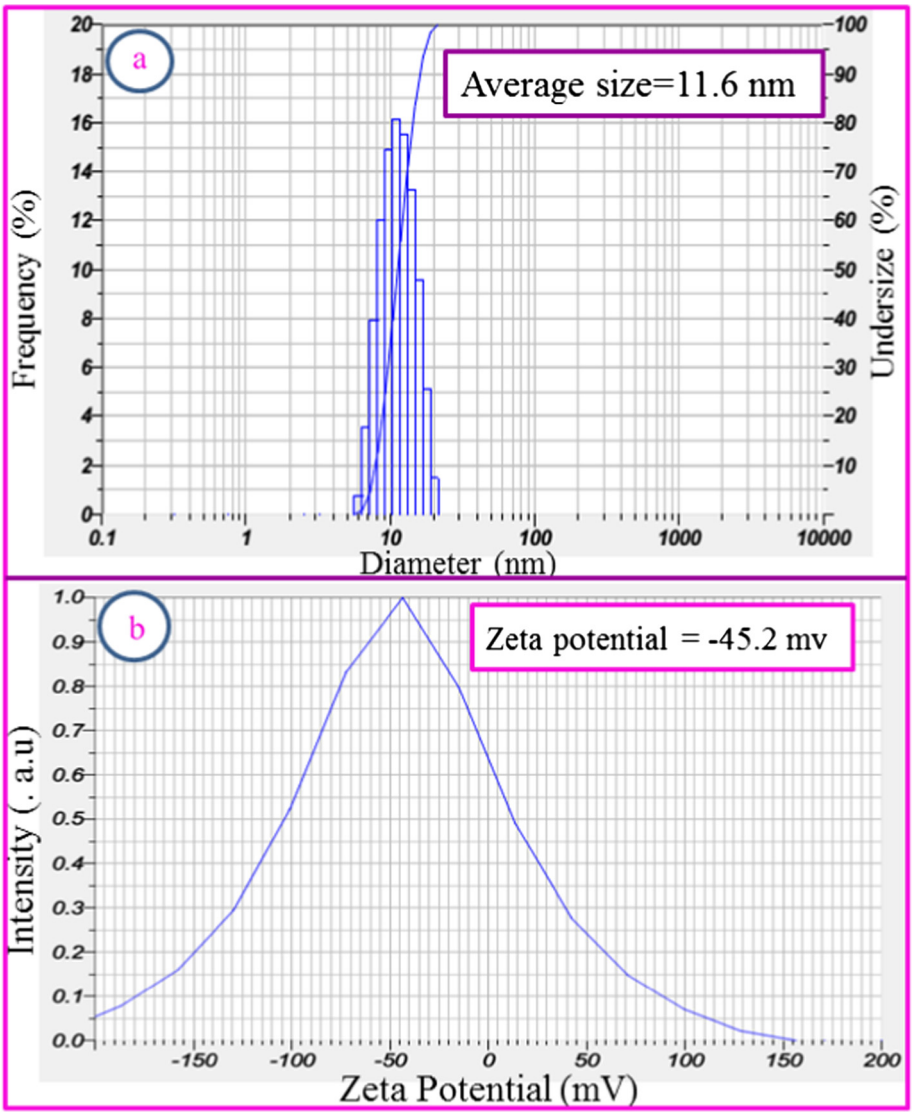

Fig. 5. DLS measurement of (a) average particle size distribution and (b) zeta potential of synthesized ZnO NPs.

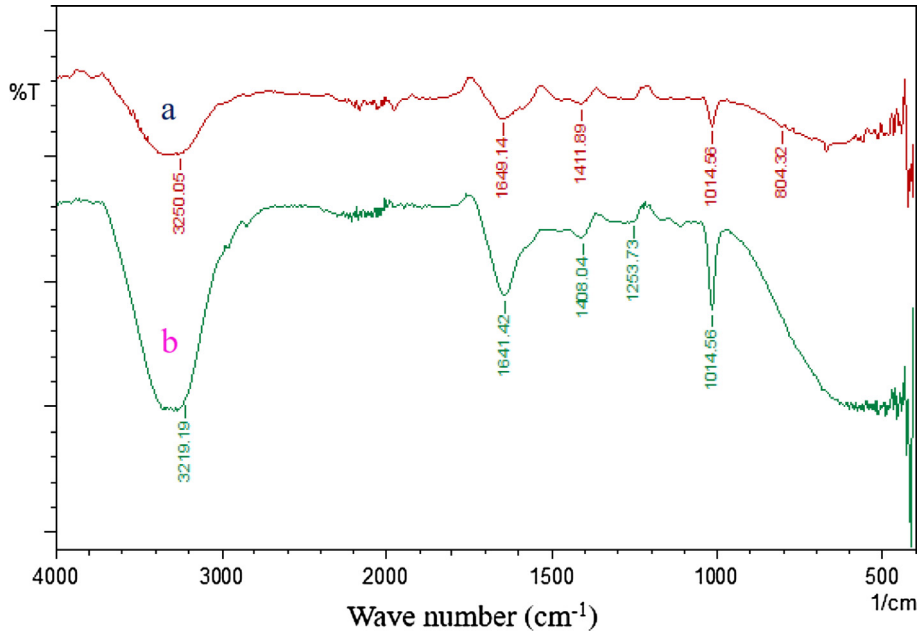

Fig. 6. FT-IR spectra of (a) synthesized ZnO NPs and (b) *Eucalyptus globulus* plant extract.

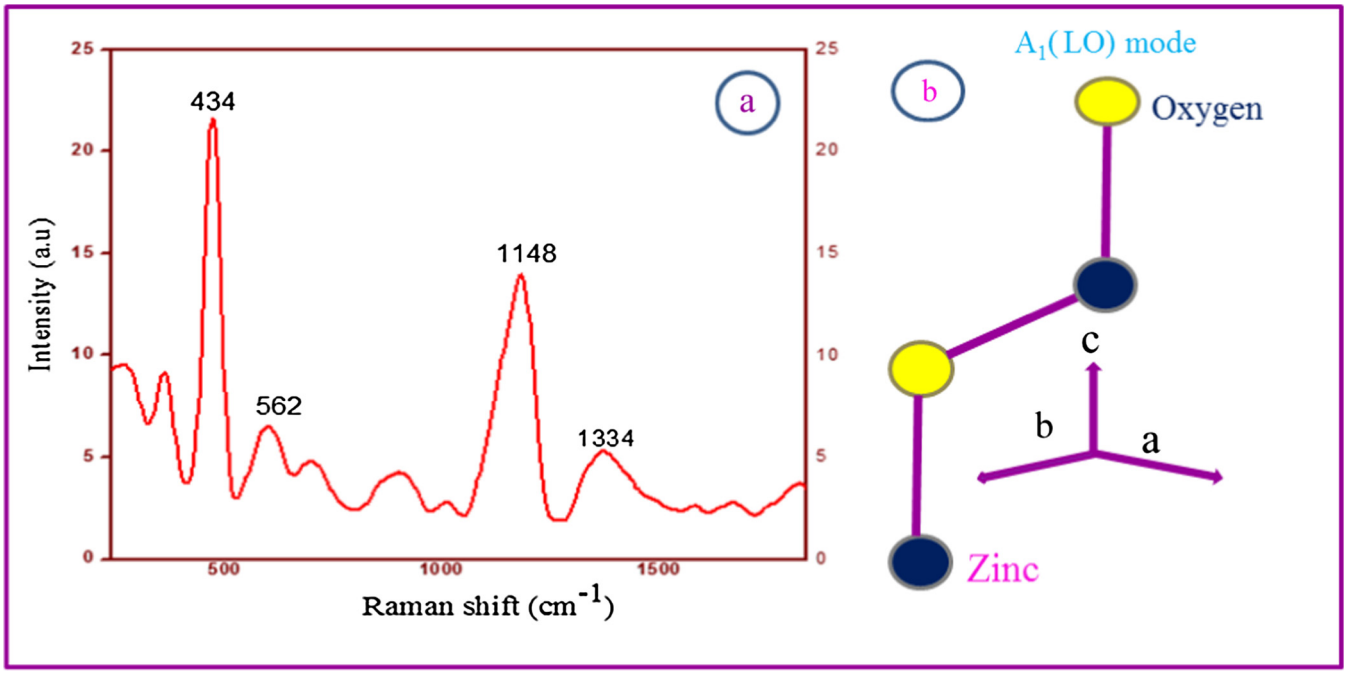

Fig. 7. Raman spectra of (a) synthesized ZnO NPs and (b) longitudinal phonon mode.

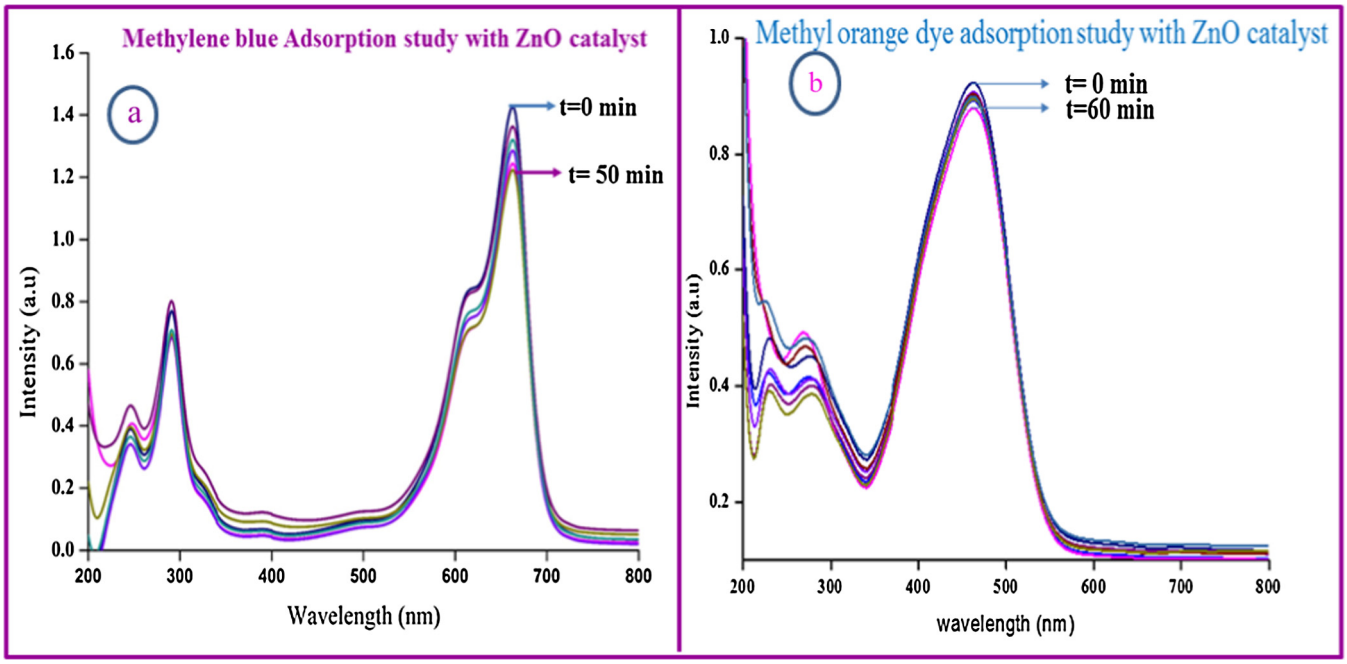

Fig. 8. UV–vis spectra for adsorption kinetics of Dyes by ZnO NPs as adsorbents in the absence of UV light irradiation (a) Methylene blue (MB) and (b) Methyl orange (MO).

different analytical instrumental methods were used to confirm the formation of ZnO NPs.

3.1. UV–visible spectroscopy study

The band gap energy of ZnO NPs was determined by UV–Visible Diffuse Reflectance mode (UV–Vis-DRS) study at a wavelength range of 200–800 nm. Band gap energy was calculated by using the following equation $\alpha = c(h\nu - E_{bulk})^{1/2}/h\nu$, where α is absorption coefficient, c is constant, $h\nu$ is the photon energy and E_{bulk} is bulk 'band gap'. Fig. 1 shows obtained data replotted between $h\nu$ verses $(\alpha h\nu)^2$ by using origin 8.0 software and the band gap was obtained by the extrapolation of a linear regression on X-axis in the plot. It is 3.17 eV which is similar to the previous reports [31].

3.2. Powder X-ray Diffraction (XRD) analysis

Fig. 2 shows the XRD pattern of synthesized ZnO NPs. It shows distinctive diffraction peaks with lattice constants of a = 3.249 Å, c = 5.176 A, c/a = 1.592 Å which matches to the hexagonal Wurtzite structure of ZnO NPs. The obtained 2θ and Miller indices (hkl) values are 31.67° (100), 34.33° (002), 36.15° (101), 47.36° (102), 56.42° (110), 62.66° (103), and 67.75° (112). The lattice constants and d-spacing values are confirmed by comparing with standard

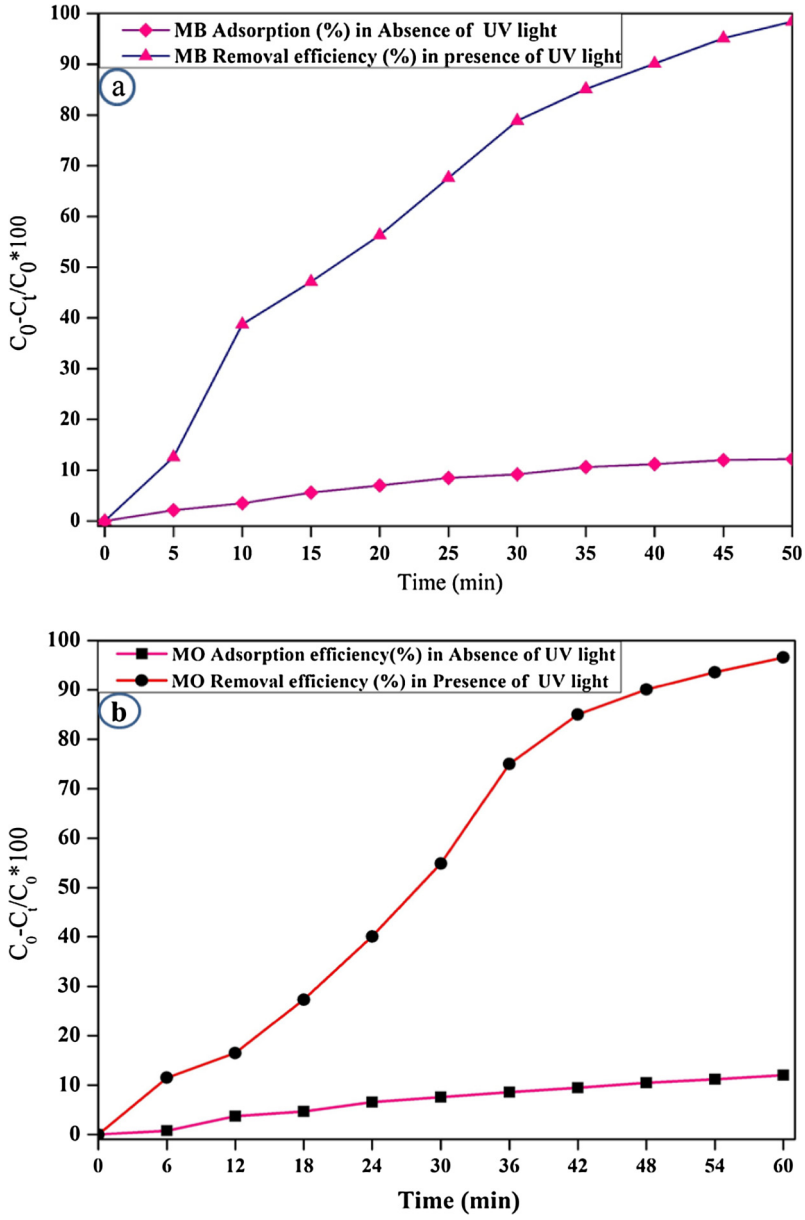

Fig. 9. Removal efficiency (%) of dyes by ZnO NPs as adsorbents (a) MB and (b) MO.

JCPDS (Joint committee on powder diffraction standards) data card no: 89-7102 [32]. The sharp and narrow diffraction peaks indicate its crystalline nature. The average diameter of crystallites (D) is calculated by using Debye-Scherer equation [33] as

$$D = \frac{0.89\lambda}{(\beta \cos\theta)},$$

where λ is the wavelength of Cu Kα radiation (1.5406 Å), β is full-width half maximum (FWHM) of (101) plane and θ is Bragg's diffraction angle. From the above Scherer, equation means crystallite size of ZnO is ~11.6 nm.

3.3. SEM and EDX analysis

Surface morphology of synthesized ZnO NPs is investigated by using field emission scanning electron microscope (FE-SEM). Fig. 3a and b clearly show that particles are almost spherical and hexagonal shape with clear separation i.e. very less agglomeration. It is similar to the results of biosynthesized ZnO NPs reported elsewhere [34]. Energy dispersive X-ray spectrum (EDX) recorded in the spot profile mode from one of the densely populated regions of ZnO NPs (Fig. 3c). EDX spectrum shows the chemical composition of synthesized ZnO NPs with strong signals from Zinc and Oxygen atoms and carbon atom at a very low intensity which confirms its purity i.e. free from impurities. The atomic and weight percentage of zinc, oxygen and carbon atoms are 40.21 (74.43%), 46.42 (21.03%) and 13.3 (4.55%), respectively.

3.4. Transmission electron microscopy (TEM) analysis

Size, shape and morphology of synthesized ZnO NPs were analyzed by TEM and high-resolution TEM (HR-TEM). Fig. 4a and b shows the TEM images at different magnifications and selective area electron diffraction (SAED) pattern which gives clear information about crystallinity and indexing with interplanar distance i.e. fringe spacing. ZnO particles are spherical in shape and size ranges from 10 to 20 nm (Fig. 4a and b). Fig. 4c shows fringe spacing as

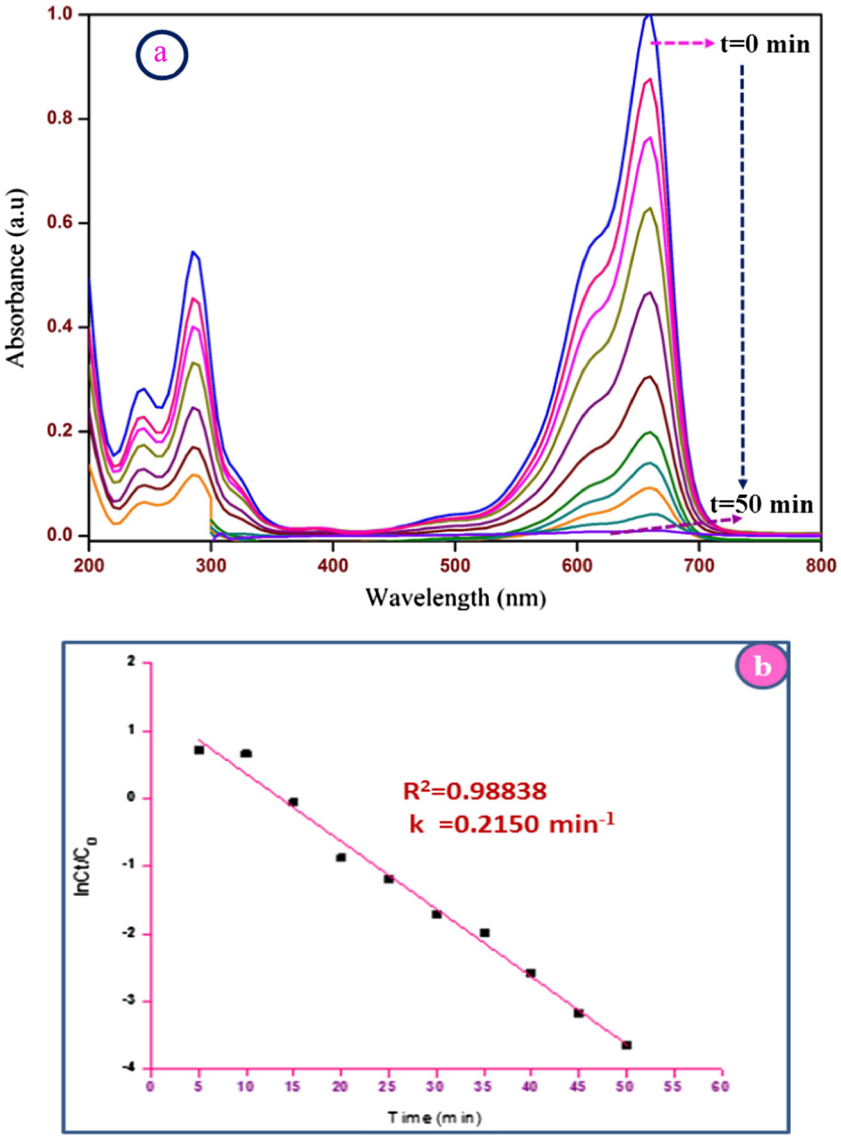

Fig. 10. Photocatalytic activity of ZnO NPs (a) plot of absorbance vs. wavelength for the decolorization of methylene blue under UV-light irradiation and (b) its first order kinetics.

2.41 Å which is in close agreement with JCPDS data card no: 89-7102 of ZnO NPs.

3.5. Particle size analysis (PSA) and zeta potential study

Dynamic light scattering (DLS) studies are used to determine the particle size distribution and average particle size of ZnO NPs at a scattering angle of 173°. The average particle size of ZnO NPs is ~11.6 nm which supports the XRD and TEM results (Figs. 2, 4a, 5a). Average zeta potential value is −45.2 mV which confirms the higher stability of ZnO NPs (Fig. 5b). The higher negative value reveals that the phytochemicals of *E. globulus* are acidic (extract pH 5.2) and provides more stability at the persistent long period of time.

3.6. Fourier transform infrared spectroscopy (FT-IR) study

FT-IR spectroscopic analysis was used to know the phytochemicals present in plant extracts responsible for the reduction of Zn^{2+} ions and stabilization of ZnO NPs. Fig. 6a and b shows the multifunctional behavior of phytochemicals of *E. globulus* before and after synthesis of ZnO NPs. The major peaks present in *E. globulus* extracts show a broad band at 3250.05 cm^{-1} due to O—H stretching of polyphenols. The next band at 1619 cm^{-1} corresponds to surface hydroxyl group of H_2O molecule, the slender band at 1411.89 cm^{-1} due to the presence of tertiary alcohol (C—OH) group. The small narrow absorption band at 1014.56 cm^{-1} represents the C—O stretching vibrations of carboxylic acids (COOH). The weaker band at 804.32 cm^{-1} is due to C—Cl stretching of alkyl halides. The FT-IR spectrum of dried ZnO NPs shows prominent capping of phytochemicals on the surface of ZnO NPs (Fig. 5a) and *Eucalyptus* leaves extract (Fig. 5b).

3.7. Raman spectroscopy study

Raman spectroscopy is a scattering technique to determine structural defects and disorders in nanostructured materials [35]. Normally, Raman peaks represent the longitudinal phonon (LO) modes and multiple harmonics A_1 (LO) mode corresponding to Raman Rayleigh spectrum of ZnO NPs (Fig. 7a). The obtained peak values at 434 cm^{-1} and 562 cm^{-1} in lower wavelength region arise due to acoustic combinations. The peak obtained at 434 cm^{-1} is the

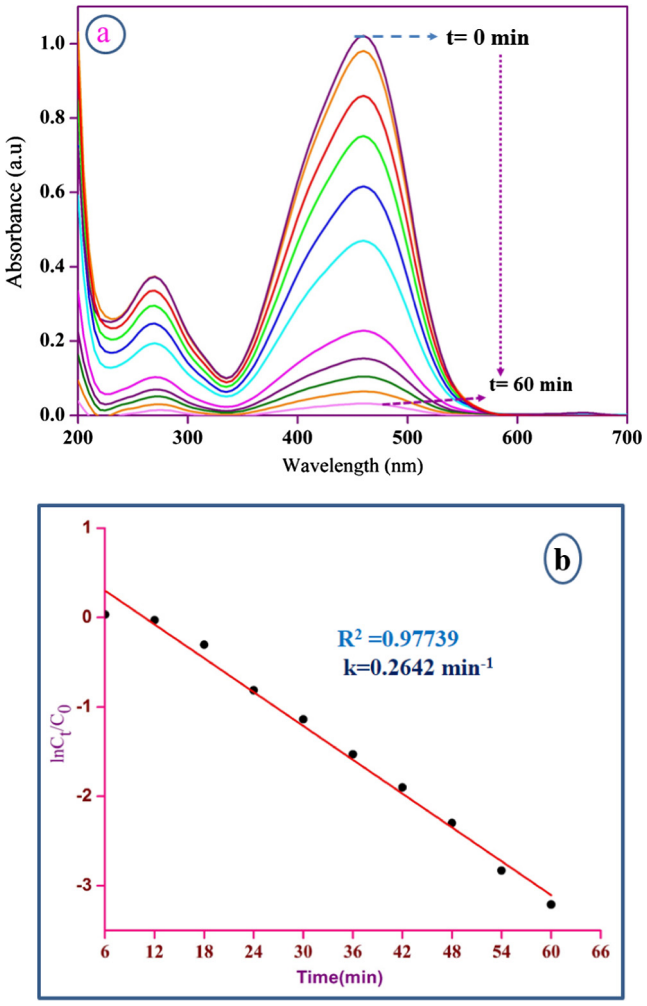

Fig. 11. Photocatalytic activity of ZnO NPs (a) plot of absorbance vs. wavelength for the decolorization of methyl orange under UV-light irradiation and (b) its first order kinetics.

characteristic first order mode of ZnO and the intermediate frequency region peak at 1148 cm^{-1} corresponds to second-order harmonics of longitudinal mode, while the origin of the peak at 1334 cm^{-1} relates to the third harmonics of longitudinal mode. Fig. 7b represents the origin of these longitudinal modes due to the displacement of zinc and oxygen atoms parallel to the *C*-axis [36].

3.8. Gas chromatography–mass spectrometry (GC–MS) study

E. globulus consists of many phytochemicals such as monoterpenes, sesquiterpenes which are identified based on peaks matching with NIST 2008 library (Table ST1). Medicinal florae containing monoterpenes are the major chemical constituents having properties like anti-inflammatory, antioxidant, analgesic and antimicrobial activity [37]. Fig. S1 shows the GC–MS chromatogram of *E. globulus* extracts containing major compounds such as Thujospene-13 (10.15%), 2-naphthalene methanol (9.67%), β-sitosterol (5.740%), benzoic acid (5.23%), α-phellandrene (4.99%), eucalyptol (3.77%) and others.

3.9. Adsorption study of methylene blue (MB) and methyl orange (MO) dyes

Fig. 8a and b represents UV–visible spectra for adsorption kinetics of MB and MO dyes at different time intervals with adsorbent ZnO NPs, whereas Fig. S2a and S2b represents UV–visible spectra for adsorption kinetics of MB and MO dyes at different time intervals without adsorbent ZnO NPs in the absence of UV light respectively. Fig. 9a and b reports the kinetic studies of both dyes plotted at different time intervals on the *X* axis and removal efficiency (%) on the *Y* axis. The removal efficiency is calculated using the following equation:

$$\text{eff} = \frac{C_0 - C_t}{C_0 * 100},$$

where C_0 = Absorbance value of dye at $t = 0$ min, C_t = Absorbance value of dye at different time t min. MB dye is removed by adsorption on the surface of catalyst up to 12% within 50 min and MO dye is removed by adsorption on the surface of catalyst up to 12.2% within 60 min in the absence of UV light irradiation. Hence UV light exposure study was carried out to check whether removal of dyes by photodegradation is influenced by photoactive ZnO NPs or not.

3.10. Photocatalytic activity of ZnO NPs

One of the major applications of metal oxide nanoparticles involved in environmental protection is their photocatalytic applications.

(a) Photocatalytic degradation of methylene blue (MB) dye

The photocatalytic activity of green synthesized ZnO NPs is checked in degrading MB dye under UV light (λ = 254 nm) irradiation. Fig. 10a elucidates the UV–visible spectra for degradation kinetics of MB at different time intervals (from 0 to 50 min) at λ_{max} of 658 nm. It clearly shows that the concentrations of MB dye decreased with time in the presence of ZnO NPs under UV light exposure. Initial cons. of MB dye solution degraded up to 98.2% after 50 min of UV illumination (Fig. 10b). However, the color of MB dye did not change significantly (~only 12.2% disappearance) when the reaction was performed for a time period of 50 min in the presence of ZnO NPs without UV light irradiation. MB dye degradation occurred up to 98.2% within 50 min irradiation time and appeared no intermediate product in the UV–visible spectrum. It clearly indicates that about 86% of the dye photodegraded more during the same time period under UV light exposure. Fig. 10b represents the plot of $\ln(C_t/C_0)$ on *Y*-axis versus irradiation time on *X*-axis which exhibits a linear relationship based on the following equation:

$\ln(C_t/C_0) = -kt$, where C_0 is a concentration of dye at time $t = 0$ min, C_t is a concentration of dye at particular time t and k is first order rate constant. Slope value obtained for MB dye is $k = 0.2997$ min^{-1} which follows first order rate kinetics.

(b) Photocatalytic degradation of Methyl Orange (MO) dye

Fig. 11a represents the photocatalytic degradation of MO dye by using ZnO NPs as a catalyst. The λ_{max} of methyl orange in UV–visible spectrum is ~460 nm. However, the color of MO dye did not change significantly (~only 12% disappearance) when the reaction was performed for a time period of 1 h without UV light irradiation. The MO dye degradation occurred up to 96.6% within 1 h irradiation time and appeared no intermediate product in the UV–visible spectrum. It clearly indicates that about 84.6% of the dye photodegraded more during the same time under UV light exposure. Although both the dyes are adsorbed on the ZnO NPs surfaces by about 12% without UV exposure, UV light exposure photodegraded the dyes manifolds i.e. by 84–86% more at the same time period.

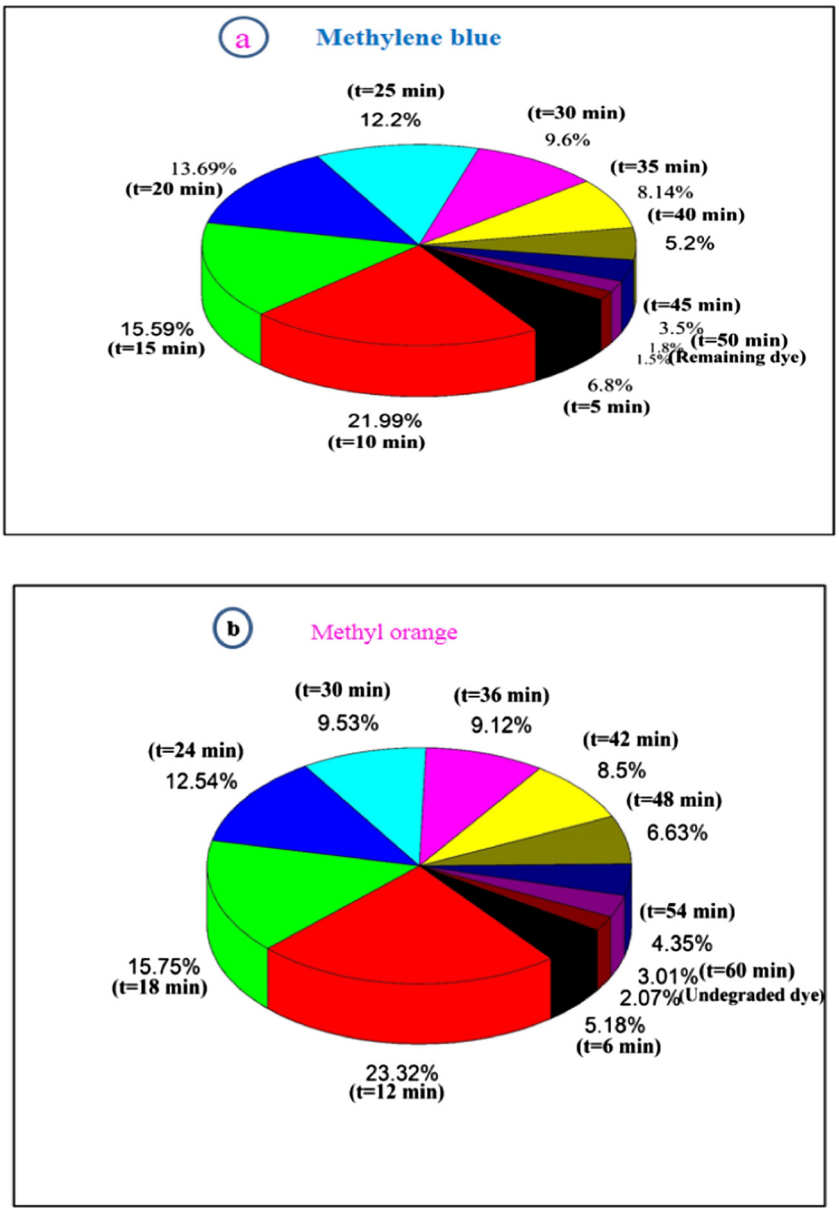

Fig. 12. Pie chart of total degradation pattern (% of photodegradation vs. time) of (a) methylene blue and (b) methyl orange dyes.

Fig. 11b shows first order kinetics of MO with rate constant k as 0.264 min^{-1}. Photocatalytic degradation efficiency of both MB and MO dyes are calculated by using the following equation as Efficiency (%) of photodegradation

$$\text{eff}(\%) = \frac{C_0 - C}{C_0 * 100},$$

where C_0 is the initial concentration of the dye solution, C is a residual concentration of the dye in solution after degradation in equilibrium. Fig. 12a and b shows the pie-chart of total degradation rate (% of photodegradation during a particular time period) of MB and MO dyes respectively.

Specific surface area and pore size distribution of synthesized catalysts are measured through adsorption and desorption isotherm of nitrogen molecules [38]. The BET specific surface area of the synthesized ZnO NPs is 38.7894 $m^2\,g^{-1}$ (Fig. S1), while the total pore volume and average pore diameter are 0.1253 $cm^3\,g^{-1}$ and 12.9216 nm respectively (Fig. S1). As same ZnO NPs is used for catalytic degradation of MB and MO, the difference in photodegradation efficiency can be explained by their absorption maxima (λ_{max} 658 nm vs. 460 nm). After exposure to same UV light MB is degraded at lower energy while compared to MO and hence slightly higher photodegradation is observed for MB (86%) compared to MO (84.4%) (Figs. 10 and 11).

The following steps are actively involved in the photodegradation of both MB and MO dyes [39].

$$ZnO + h \rightarrow e^- + h^+ \quad (1)$$

$$h^+ + H_2O \rightarrow O\dot{H} + H^+ \quad \text{Or} \quad (2)$$

$$OH^- + h^+ \rightarrow OH^{\cdot} \quad (3)$$

$$O_2 + e^- \rightarrow \dot{O}_2^- \quad (4)$$

$$\dot{O}_2^- + H^+ \rightarrow O\dot{O}H \quad (5)$$

$$ZnO(e^-) + \dot{O}_2^- + 2H^+ \rightarrow ZnO + H_2O_2 \quad (6)$$

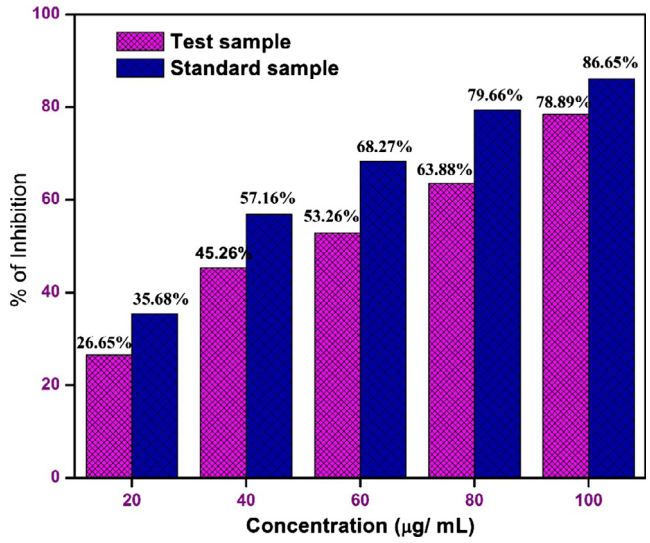

Fig. 13. Antioxidant activity of different concentrations (25, 50, 75, 100 μg/ml) of synthesized ZnO NPs by DPPH scavenging assay.

$$ZnO(e^-) + H_2O_2 \rightarrow ZnO + O\dot{H} + OH^- \quad (7)$$

$$Dye + \{O_2, O_2^-, O\dot{O}H\} \rightarrow \text{Mineralized Product} \quad (8)$$

The active oxygen species (O_2, O_2^-) and hydroxyl free radicals (·OH, OOH·) are effectively involved in the degradation of organic pollutants in waste water into less harmful minerals CO_2 and H_2O. These results reveal that the photocatalyst ZnO NPs are highly suitable for environmental purification processes.

3.11. Antioxidant activity by DPPH scavenging assay method

In pharmaceutical science as well as nanoscience and technology the investigation of antioxidant activity plays a significant role. Banerjee et al. [40] compared antioxidant activity of bulk and nanostructured materials. Green synthesized ZnO NPs showed enhanced antibacterial and antioxidant activity due to the capping of major chemical compounds on the surface of nanoparticles [41]. Cuminic aldehyde and β-Sitosterol being major phytochemicals in the extracts influenced the antioxidant activity [42], while esters and ethyl palmitate showed anti-inflammatory activity [43]. Edris et al. explained that 1, 8 cineole and thymol of *E. globulus* were major polyphenol constituent responsible for stronger antioxidant activity [44].

Previous reports investigated that both NiO and Fe_3O_4 NPs exhibited good antioxidant activity [45,46]. Banerjee et al. performed activity studies of bulk and nanostructured ZnO materials and found that nanomaterials showed higher free radical scavenging capacity compared to bulk materials due to its high surface to volume ratio [47]. In the present study ZnO NPs dispersion with varying concentrations (20, 40, 60, 80, 100 μg/mL) were prepared in methanol and added to 1 mM (10^{-3}N) DPPH in a small test tube and incubated at 37 °C for 30 min under dark conditions. The color change from blue to yellow was monitored by a UV–visible spectrophotometer at a λ_{max} of 517 nm. Ascorbic acid was taken as standard reference antioxidant material for this study. The percentage of scavenging capacity was measured by using the following formula:

$$\text{Percentage}(\%)\text{of DPPH scavenging inhibition} = (A_0 - A_t)/A_0 \times 100,$$

where A_0, A_t are absorbance values of control (DPPH) sample and test sample (DPPH with different dosage of ZnO NPs). Fig. 13 represents the antioxidant activity of standard ascorbic acid and test samples at various concentrations (μg/mL) on *X*-axis and percentage of scavenging inhibition on *Y*-axis. All the samples were tested in triplicate for concordant results. ZnO NPs exhibited up to 82% of scavenging capacity with IC_{50} value as 46.62% μg/mL (Fig. S3). Antioxidant activity of ZnO NPs ascribed due to smaller particle grain size (11.6 nm) and other reason may be a phenomenon of transfer of electron density from Oxygen atom to odd electron located at nitrogen atom in DPPH which results in decreasing $n \rightarrow \pi^*$ transition intensity at 517 nm [48]. Fig. 14 signifies the mechanism of antioxidant activity in which unstable blue colored methanolic DPPH solution turns to stable yellow color with addition of different dosage of antioxidant ZnO NPs due to its scavenging activity of DPPH free radicals by donation of electron on oxygen atom to the odd electron of nitrogen atom resulting the formation of stable DPPH molecule [49,50]. In other words, the antioxidant activity depends on its hydrogen donation capacity. In addition, large numbers of electrons and holes pair formation on ZnO NPs surface even in the absence of UV light creates a high redox

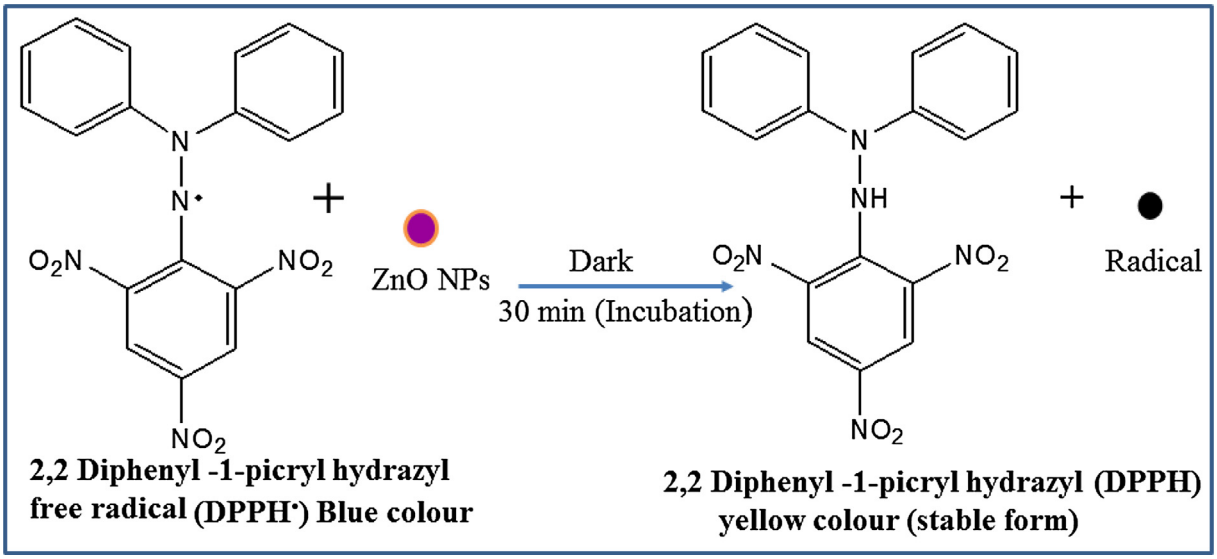

Fig. 14. Mechanistic representation of interaction between DPPH free radicle and ZnO NPs forming stable DPPH molecule.

potential that splits water into hydroxyl and hydrogen radicals [51] which is available for DPPH free radical reduction and stability of DPPH molecule.

4. Conclusions

In summary, we report a facile and efficient method to synthesize spherical ZnO NPs by hydrothermal method using a *E. globulus* extract as reducing and capping agent. The synthesized ZnO NPs was characterized by XRD and its pattern was indexed to hexagonal wurtzite structure with average crystallite size of 11.6 nm which was supported by DLS study. The spherical shape and particle size ranges of 10–16 nm were confirmed by TEM results. Zeta potential was −45.2 mV which shows its high stability for a longer period. Multifunctional groups involved in extracts and functional groups capped on the surface of ZnO NPs are confirmed by FT-IR studies. The ZnO NPs exhibited efficient photocatalytic activity in degrading MB and MO dyes under UV light exposure. This is the first report on the degradation of organic dyes MB and MO by using ZnO NPs as a catalyst. Synthesized ZnO NPs also exhibited high antioxidant activity against DPPH molecule compared to ascorbic acid as standard reference material. Hence the present study significantly demonstrates a facile eco-friendly method to synthesize ZnO NPs which may be the best substitute for both physical and chemical methods.

Acknowledgements

The authors gratefully acknowledge to VIT University, Vellore for providing a platform and basic characterization facility to do this work. Also, sincerely thankful to UGC-NRC (Networking resource center) of School of Chemistry, University of Hyderabad for providing all necessary facilities and Centre for Nanotechnology research for providing Photoreactor and TEM facility for carrying out this work.

Appendix A. Supplementary material

Supplementary data associated with this article can be found, in the online version, at http://dx.doi.org/10.1016/j.apt.2016.11.026.

References

[1] D. Sannino, V. Vaiano, O. Sacco, P. Ciambelli, Mathematical modelling of photo catalytic degradation of methylene blue under visible light irradiation, J. Environ. Chem. Eng. 1 (2013) 56–60.
[2] P.B.S. Ratna, Pollution due to synthetic dyes toxicity and carcinogenicity studies and remediation, Int. J. Environ. Sci. 3 (2012) 940–955.
[3] J. McCann, B.N. Ames, Detection of carcinogens as mutagens in the Salmonella/microsome test: assay of 300 chemicals, Proc. Natl. Acad. Sci. U.S.A. 73 (1976) 950–954.
[4] L. Liqin, W. Wenta, H. Jiale, L. Qingbiao, S. Daohua, Y. Xin, W. Huixuan, H. Ning, W. Yuanpeng, Plants: emerging as green source toward biosynthesis of metallic nanoparticles and its applications, J. Bioprocess. Chem. Eng. 2 (2014) 2348–3768.
[5] K.-T. Lee, X.-F. Chuah, Y.-C. Cheng, S.-Y. Lu, Pt coupled $ZnFe_2O_4$ nano crystals as a breakthrough photo catalyst for Fenton-like processes–photo degradation treatments from hours to seconds, J. Mater. Chem. A 3 (2015) 18578–18585.
[6] X.D. Wang, J. Song, J. Liu, Z.L. Wang, Direct-current nano generator driven by ultrasonic waves, Science 316 (2007) 102–105.
[7] R. Chauhan, A. Kumar, R. Chaudhary, Structure and optical properties of $Zn_{1-x}NiO_x$ nanoparticles by co-precipitation method, J. Optoelectron. Biomed. Mater. 3 (2011) 17–23.
[8] S. Ameen, M.S. Akhtar, Y.S. Kim, H.S. Shin, Semiconducting nanostructures and nano composites for the recognition of toxic chemicals, Appl. Catal. B: Environ. 103 (2011) 136–142.
[9] S. Dawood, T.K. Sen, Adsorption kinetics of bromophenol blue and eriochrome black t using bentonite carbon composite material, Int. J. Sci. Eng. Res. 6 (2015) 2229–5518.
[10] K. Ellmer, Past achievements and future challenges in the development of optically transparent electrodes, Nat. Photonics 6 (2012) 809–817.
[11] V.V. Ursaki, I.M. Tiginyanu, V.V. Zalamai, E.V. Rusu, G.A. Emelchenko, V.M. Masalov, E.N. Samarov, Phys. Rev. B 70 (2004) 155204-1–155204-8.
[12] S. Ameen, M.S. Akhtar, H.S. Shin, Highly dense ZnO nanowhiskers for the low level detection of p-Hydroquinone, Mater. Lett. 155 (2015) 82–86.
[13] Y. Chen, S. Ma, Preparation and photoluminescence studies of high-quality AZO thin Films grown on ZnO buffered Si substrate, Mater. Lett. 162 (2016) 75–78.
[14] F. Fan, Y. Feng, P. Tang, D. Li, Facile synthesis and photo catalytic performance of ZnO nanoparticles self-assembled spherical aggregates, Mater. Lett. 158 (2015) 290–294.
[15] R. Suntako, Effect of synthesized ZnO Nano grains using a precipitation method for the Enhanced cushion rubber properties, Mater. Lett. 158 (2015) 399–402.
[16] T.X. Wang, S.H. Xu, F.X. Yang, Green synthesis of CuO Nanoflakes from $CuCO_3{\cdot}Cu(OH)_2$ powder and H_2O_2 aqueous solution, Powder Technol. 228 (2012) 128–130.
[17] O. Carpa, A. Tirsoaga, B. Jurca, R. Ene, Simona Somacescu, Adelina Ianculescu, Biopolymer starch mediated synthetic route of multispheres and donut ZnO structures, Carbohydr. Polym. 115 (2015) 285–293.
[18] S. Zhao, D. Zhang, Supercritical CO_2 extraction of Eucalyptus leaves oil and comparison with soxhlet extraction and hydro-distillation methods, Sep. Purif. Technol. 133 (2014) 443–451.
[19] K. Elumalai, S. Velmurugan, Green synthesis, characterization and antimicrobial activities of zinc oxide nanoparticles from the leaf extract of *Azadirachta indica* (L.), Appl. Surf. Sci. 345 (2015) 329–336.
[20] W. Brand Williams, Protein extraction from plant tissue in methods in molecular biology, protein purification protocols, Food Sci. Technol. 28 (1995) 23–30.
[21] A. Kołodziejczak-Radzimska, T. Jesionowski, A. Krysztafkiewicz, Obtaining zinc oxide from aqueous solutions of KOH and Zn $(CH_3COO)_2$, Physicochem. Probl. Miner. Process. 44 (2010) 93–102.
[22] J.-H. Park, Y.-J. Choi, J.-G. Park, Synthesis of ZnO nanowires and nanosheets by an O_2^- assisted carbothermal reduction process, J. Cryst. Growth 280 (2005) 161–167.
[23] T.T. Ali, K. Narasimharao, I.P. Parkin, C.J. Carmalt, S. Sathasivam, S.N. Basahel, S. M. Bawaked, S.A. Al-Thabaiti, Effect of pretreatment temperature on the photocatalytic activity of microwave irradiated porous nanocrystalline ZnO, New J. Chem. 39 (2015) 321–332.
[24] S. Musić, Đ. Dragčević, S. Popović, M. Ivanda, Precipitation of ZnO particles and their properties, Mater. Lett. 59 (2005) 2388–2393.
[25] D. Visinescu, M. Scurtu, R. Negrea, R. Birjega, D.C. Culita, M.C. Chifiriuc, C. Draghici, J.C. Moreno, A.M. Musuc, I. Balint, Additive-free 1,4-butanediol mediated synthesis: a suitable route to obtain nanostructured, mesoporous spherical zinc oxide materials with multifunctional properties, RSC Adv. 5 (2015) 99976–99989.
[26] E.K. Goharshadi, Y. Ding, P. Nancarrow, Green synthesis of ZnO nanoparticles in a room-temperature ionic liquid 1-ethyl-3-methylimidazolium bis (trifluoromethylsulfonyl) imide, J. Phys. Chem. Solids 69 (2008) 2057–2060.
[27] F. Thema, E. Manikandan, M.S. Dhlamini, M. Maaza, Green synthesis of ZnO nanoparticles via Agathosma betulina natural extract, Mater. Lett. 161 (2015) 124–127.
[28] K. Manjunath, T. Ravishankar, D. Kumar, K. Priyanka, T. Varghese, H.R. Naika, H. Nagabhushana, S. Sharma, J. Dupont, T. Ramakrishnappa, Facile combustion synthesis of ZnO nanoparticles using *Cajanus cajan* (L.) and its multidisciplinary applications, Mater. Res. Bull. 57 (2014) 325–334.
[29] T. Karnan, S.A.S. Selvakumar, Biosynthesis of ZnO nanoparticles using rambutan (*Nephelium lappaceum* L.) peel extract and their photocatalytic activity on methyl orange dye, J. Mol. Struct. 1125 (2016) 358–365.
[30] J. Fowsiya, G. Madhumitha, N.A. Al-Dhabi, M.V. Arasu, Photocatalytic degradation of Congo red using *Carissa edulis* extract capped zinc oxide nanoparticles, J. Photochem. Photobiol. B: Biol. 162 (2016) 395–401.
[31] C. Chinnarasua, A. Montes, M.T. Fernandez-Poncea, L. Casas, C. Mantell, C. Pereyraa, E.J. Martinez de la Ossaa, S. Pattabhi, Natural antioxidant fine particles recovery from *Eucalyptus globulus* leaves using supercritical carbon dioxide assisted processes, J. Supercrit. Fluids 101 (2015) 161–169.
[32] S. Monticone, R. Tufeu, A.V. Kanaev, Complex nature of the UV and visible–fluorescence of colloidal ZnO nanoparticles, J. Phys. Chem. B 102 (1990) 2854–2862.
[33] P.D. Duh, Z.T. Chen, S.W. Lee, T.P. Lin, Y.T. Wang, W.J. Yen, L.F. Kuo, H.L. Chu, Antiproliferative activity and apoptosis induction of Eucalyptus Citriodora resin and its major bioactive compound in melanoma B16F10 cells, J. Agric. Food Chem. 60 (2012) 7866–7872.
[34] C. Jayaseelan, A. AbdulRahuman, A. Vishnu, S. Kirthi, T. Marimuthu, T. Santhoshkumar, A. Bagavan, K. Gaurav, L. Karthik, K.V. Bhaskara Rao, Spectrochim. Acta Part A 90 (2012) 78–84.
[35] P. Rajiv, S. Rajeshwari, R. Venckatesh, Bio-Fabrication of zinc oxide nanoparticles using leaf extract of *Parthenium hysterophorus* L. and its size-dependent antifungal activity against plant fungal pathogens, Spectrochim. Acta, Part A 112 (2013) 384–387.
[36] Q.I. Rahman, M. Ahmad, S.K. Misra, M. Lohani, Effective photo catalytic degradation of rhodamine B dye by ZnO nanoparticles, Mater. Lett. 91 (2013) 170–174.
[37] T. Wu, G. Liu, J. Zhao, H. Hidaka, N. Serpone, Photo assisted degradation of dye pollutants self-photosensitized oxidative transformation of Rhoda mine B under visible light irradiations in aqueous TiO_2 dispersions, J. Phys. Chem. B 102 (1998) 5845–5851.

[38] C. Tamuly, I. Saikia, M. Hazarika, M. Bordoloi, N. Hussain, M.R. Das, K. Deka, Bio-derived ZnO nanoflower: a highly efficient catalyst for the synthesis of chalcone derivatives, RSC Adv. 5 (2015) 8604–8608.
[39] D. Roberto, P. Micucci, T. Sebastian, F. Graciela, C. Anesini, Antioxidant activity of limonene on normal murine lymphocytes: relation to H_2O_2 modulation and cell proliferation, Clin. Pharmacol. Toxicol. 106 (2010) 38–44.
[40] S. Banerjee, J.P. Saikia, A. Kumar, B.K. Konwar, Antioxidant activity and haemolysis prevention efficiency of polyaniline nanofibers, Nanotechnology 21 (2010) 045101, http://dx.doi.org/10.1088/0957-4484/21/4/045101, Epub 2009 Dec 10.
[41] F. Ayoughi, M. Marzegar, A.M. Sahari, H. Naghdibadi, Chemical compositions of essential oils of *Artemisia dracunculus* L. and endemic *Matricaria chamomilla* L. and an evaluation of their antioxidative effects, J. Agric. Food Chem. 1 (2011) 79–88.
[42] A.G. Guimarães, J.S.S. Quintans, J.L. Quintans-Júnior, Monoterpenes with analgesic activity a systematic review, Photother. Res. 27 (2013) 1–15.
[43] K. Mwangi, M. Ndungu, L. Gitu, Repellent activity of the essential oil from Capparis tomentosa against maize weevil Sitophilus zeamais, J. Resour. Dev. Manage. 1 (2013) 9–13.
[44] A.E. Edris, Pharmaceutical and therapeutic potentials of essential oils and their individual volatile constituents: a review, Photother. Res. 4 (2007) 308–323.
[45] S. Paul, J.P. Saikia, B.K. Konwar, S.K. Samdarshi, Investigation of antioxidant property of iron oxide particles by 1–10 diphenylpicryl-hydrazyle (DPPH) method, J. Magn. Mater. 321 (2009) 3621–3623.
[46] J.P. Saikia, S. Paul, B.K. Konwar, S.K. Samdarshi, Nickel oxide nanoparticles: a novel antioxidant, Colloids Surf. B: Biointerfaces 268 (2010) 146–148.
[47] D. Dasa, B. Chandra, N.P. Phukonc, A. Kalitaa, S.K. Doluia, Surface area to volume ratios of ZnO NPs are responsible for significant higher antibacterial activities, Colloids Surf. B: Biointerfaces 111 (2013) 556–560.
[48] H.R. Madan, S.C. Sharma, U. dayabhanu, D. Suresh, Y.S. Vidya, H. Nagabhushana, H. Rajanaik, K.S. Anantharaju, S.C. Prashantha, P. Sadananda Maiya, Facile green fabrication of nanostructure ZnO plates, bullets, flower, prismatic tip, closed pine cone: their antibacterial, antioxidant, photo luminescent and photo catalytic properties, Spectrochim. Acta Part A: Mol. Biomol. Spectrosc. 152 (2015) 404–416.
[49] L. Sun, J. Zhang, X. Lu, L. Zhang, Y. Zhang, Evaluation to the antioxidant activity of total flavonoids extract from persimmon (*Diospyros kaki* L.) leaves, Food Chem. Toxicol. 49 (2011) 2689–2696.
[50] H.A. Kiran Kumar, B.K. Mandal, K. Mohan Kumar, S. Maddinedi, T. Sai Kumar, P. Madhiyazhagan, A.R. Ghosh, Antimicrobial and antioxidant activities of Mimusops elengi seed extract mediated isotropic silver nanoparticles, Spectrochim. Acta Part A Mol. Biomol. Spectrosc. 130 (2014) 13–18.
[51] H. Yang, C. Liu, D. Yang, H. Zhang, Z. Xi, Comparative study of cytotoxicity, oxidative stress and genotoxicity induced by four typical nanomaterials: the role of particle size, shape and composition, J. Appl. Toxicol. 29 (2009) 69–78.